Supplementary Information for

Crystalline-Amorphous Interfaces Enriched CuS-SnS Composite Catalyst Boosts Electrochemical CO_2 Reduction over a Wide pH Window

Shanshan Wang, [a] Baoxin Ni, [b] Wei-Yi Zhang, [a] Yanbo Hua, [a] Jia-Ao Huang, [a] Hui Fan, [a] Hong Li, [c] Songhai Xie, [a] Tian-Wen Jiang,*[a] Kun Jiang, [a] Junliang Zhang [d] and Wen-Bin Cai*[a]

a. Shanghai Key Laboratory of Molecular Catalysis and Innovative Materials, State Key Laboratory of Porous Materials for Separation and Conversion, iChEM (Collaborative Innovation Center of Chemistry for Energy Materials), Department of Chemistry, Fudan University, Shanghai 200438, China.

b. National Key Laboratory of Advanced Micro and Nano Manufacture Technology, Department of Micro/Nano Electronics, School of Electronic Information and Electrical Engineering, Shanghai Jiao Tong University, Shanghai 200240, China.

c. School of Materials and Chemistry, University of Shanghai for Science and Technology, Shanghai 200093, China.

d. Institute of Fuel Cells, School of Mechanical Engineering, Shanghai Jiao Tong University, Shanghai 200240, China.

1. Experimental section

1.1. Chemicals.

Cupric chloride dihydrate ($CuCl_2 \cdot 2H_2O$), Stannous chloride dihydrate ($SnCl_2 \cdot 2H_2O$), Potassium sulphate (K_2SO_4), Potassium bicarbonate ($KHCO_3$) and Sulfuric acid (H_2SO_4) were purchased from Sinopharm Chemical Reagent. Sodium sulfide nonahydrate ($Na_2S \cdot 9H_2O$) was purchased from Aladdin. All the reagents were used as received. All solutions were prepared with ultrapure Milli-Q water with a resistivity of 18.2 MΩ cm.

1.2. Synthesis of CuS-SnS, CuS and SnS.

For the synthesis of CuS-SnS, 2.26 g $SnCl_2 \cdot 2H_2O$ and 1.71 g $CuCl_2 \cdot 2H_2O$ were dissolved adequately in 100 mL H_2O. Afterwards, 4.80 g $Na_2S \cdot 9H_2O$ was dissolved adequately in 100 mL H_2O. Then the sodium sulfide aqueous solution was added to the mixed solution of cupric chloride and stannous chloride using a peristaltic pump at a drip rate of 4000 μL min^{-1}. Continuing the reaction at a stirring speed of 500 rpm for 5 min, the brown precipitate was collected through vacuum filtration and multiple washes with deionized water. The cooled product was obtained by drying overnight in a vacuum drying oven at 50 °C. Using the same method, 3.42 g of $CuCl_2 \cdot 2H_2O$ and 4.52 g of $SnCl_2 \cdot 2H_2O$ were respectively used to prepare CuS and SnS as the control samples.

1.3. Characterizations.

TEM, HRTEM, SAED and EDS were carried on JEM-F200 TEM at an accelerating voltage of 300 kV to determine the morphologies, sizes, element mapping and lattice fringes of catalysts. XRD measurement was conducted on a Bruker D8 Discover spectrometer equipped with a Cu radiation source (λ=0.15406 nm). SEM was operated on Nova NanoSem 450 SEM at an accelerating voltage of 200 kV. The XPS were collected by AXIS Kratos Supra+. The carbon peak at 284.8 eV was used as the

reference to correct for charging effects. The specific surface areas of the catalysts were determined by nitrogen adsorption-desorption measurements at 77 K using a Automatic Specific Surface Area and Porosimetry Analyzer (3020). Prior to analysis, the samples were degassed under high vacuum at 250 ℃ for 3 hours to remove adsorbed moisture and gases. The Brunauer-Emmett-Teller (BET) method was applied to calculate the specific surface area from the adsorption data in the relative pressure (P/P_0) range of 0 -1.

1.4. Electrochemical CO_2RR Measurement

All CO_2RR experiments were carried out in a Flow cell by Biologic VSP-300 potentiostat. The catalyst inks were prepared by ultrasonically dispersing 35 mg of catalysts in 15 mL of isopropanol, and 175 μL of 5 wt. % alkaline ionomer solution DM XA-9. This ink was sprayed onto a 3.5 cm × 4.5 cm carbon gas diffusion layer with a catalyst loading of 0.775 mg cm^{-2}. A customized flow cell reactor consisting of a 1 cm^2 GDE cathode, an IrO_2-coated Ti fiber felt anode, and a leak-free Ag/AgCl (Innovative Instruments) reference electrode. The alkaline catholyte was 1.0 M KOH solution. The neutral catholyte was 1.0 M $KHCO_3$ solution. The acidic catholyte was a mixture of 0.05 M H_2SO_4 and 0.5 M K_2SO_4 mixed solution. Furthermore, the alkaline, neutral, and acidic catholytes were measured with a pH-100 meter and yielded values of 13.28, 8.22, and 1.81, respectively. All anolytes were 0.1 M H_2SO_4. And the ion exchange membrane was used to separate anode and cathode part. During the reduction process, the flow rate of carbon dioxide was maintained at 50 sccm, and the flow rate of the electrolyte was maintained at 2 mL min^{-1}. The reaction was carried out using a constant current method, with the applied current density ranging from 100 to 1000 mA cm^{-2}. The solution resistance (R_u) was determined using potentiostatic electrochemical impedance spectroscopy (PEIS) at frequencies ranging from 0.1 Hz to 100 kHz, and manually compensated as E (iR-corrected vs. RHE) = E (vs. RHE) − Ru × i (amps of averaged current). All potentials (if not specifically mentioned) in this work were converted to the RHE scale by E (vs. RHE) = E (vs. SCE) + 0.244 V + 0.0592 × pH_{bulk}

and E (vs RHE) = E (vs. Ag/AgCl) + 0.197 V + 0.0592 × pH_{bulk}. The galvanostatic electrochemical impedance spectroscopy (GEIS) measurements were performed at 100 mA cm^{-2} within a frequency range between 1×10^5 Hz and 0.1 Hz and an AC amplitude of 10 mA.

1.5. Distribution of relaxation times

Electrochemical impedance spectroscopy (EIS) data were transformed into DRT spectra to resolve overlapping processes with similar time constants. The impedance $Z(\omega)$ is expressed as a series of RC elements:

$$Z(\omega) = R_0 + \int_0^{+\infty} \frac{g(\tau)}{1+jw\tau} d\tau \quad (1)$$

where R_0 is the ohmic resistance, τ is the relaxation time ($\tau = 1/2\pi f$), and $g(\tau)$is the distribution function. Equation (1) is reformulated as:

$$Z(\omega) = R_0 + \int_{-\infty}^{+\infty} \frac{\gamma(\tau)}{1+jw\tau} dln\tau \quad (2)$$

where $\gamma(\tau) = \tau g(\tau)$.

Due to the ill-posed nature of this inversion, Tikhonov regularization was applied to stabilize the solution [1-4]:

$$s(x) = \|Ax-b\|^2 + \|\lambda x\|^2 \quad (3)$$

Here, $\|Ax-b\|^2$ represents residuals between experimental and reconstructed impedance, λ is the regularization parameter, and x is the discretized $\gamma(\tau)$. Prior to DRT interpretation of EIS data, parametric optimization of the regularization parameter λ was performed through rigorous residual analysis. The sum of squared residuals (SSR) served as the quantitative criterion for λ selection[5]:

$$\Delta^2 = \frac{\int_{i=1}^{M} \left[\left(Res_{re,i} \right)^2 + \left(Res_{im,i} \right)^2 \right]}{\int_{i=1}^{M} |Z_{exp,i}|} \quad (4)$$

where $Res_{re,i}$ and $Res_{im,i}$ denote residuals between experimentally measured impedance ($Z_{exp,i}$) and reconstructed impedance from DRT spectra. This systematic approach ensured optimal noise suppression while preventing overfitting.

In this work, the DRT analysis was performed using an open-source MATLAB toolbox (DRT tools) from the Ciucci group, which is based on the radial basis function discretization method with Tikhonov regularization.[6] The key parameters used in the calculation are summarized in Table S1.

Table S1: Important parameters applied in DRTtools.

Parameters	**Values of parameters**
Regularization derivative	1st order
Data type for fitting	Combined Re-Im Data
Radial basis function	Gaussian, shape control (FWHM coefficient = 0.5)
Regularization parameter	1×10^{-4}

1.6. CO_2RR products quantification

The gaseous CO and H_2 product were detected by Shimadzu 2014 gas chromatography (GC) equipped with a flame ionization detector (FID) and a thermal conductivity detector (TCD). Ultra High Pressure (UHP) Ar was used as the carrier gas and constituents of the gaseous sample were separated using two Porapak N80/100 columns packed with molecular sieve-13X. Faradaic efficiency of certain reduction product *i* (FE_i) was calculated as:

$$FE_i = \frac{nFvx_i}{jtV}$$

where x_i is the volume fraction of specie i as determined by online GC, v (sccm) is the flow rate monitored by an Alicat mass flow controller, n is the number of electrons transferred, F is the Faradaic constant, V (L mol^{-1}) is the molar volume of ideal gas under CO_2RR operation condition, j (mA cm^{-2}) is the total current density, t (s) is the running time.

The liquid formate products were quantified by high performance liquid chromatography (HPLC). The FE of HCOOH was determined by dividing the charge contributed to product by the total charge passed at a given time span.

Figures

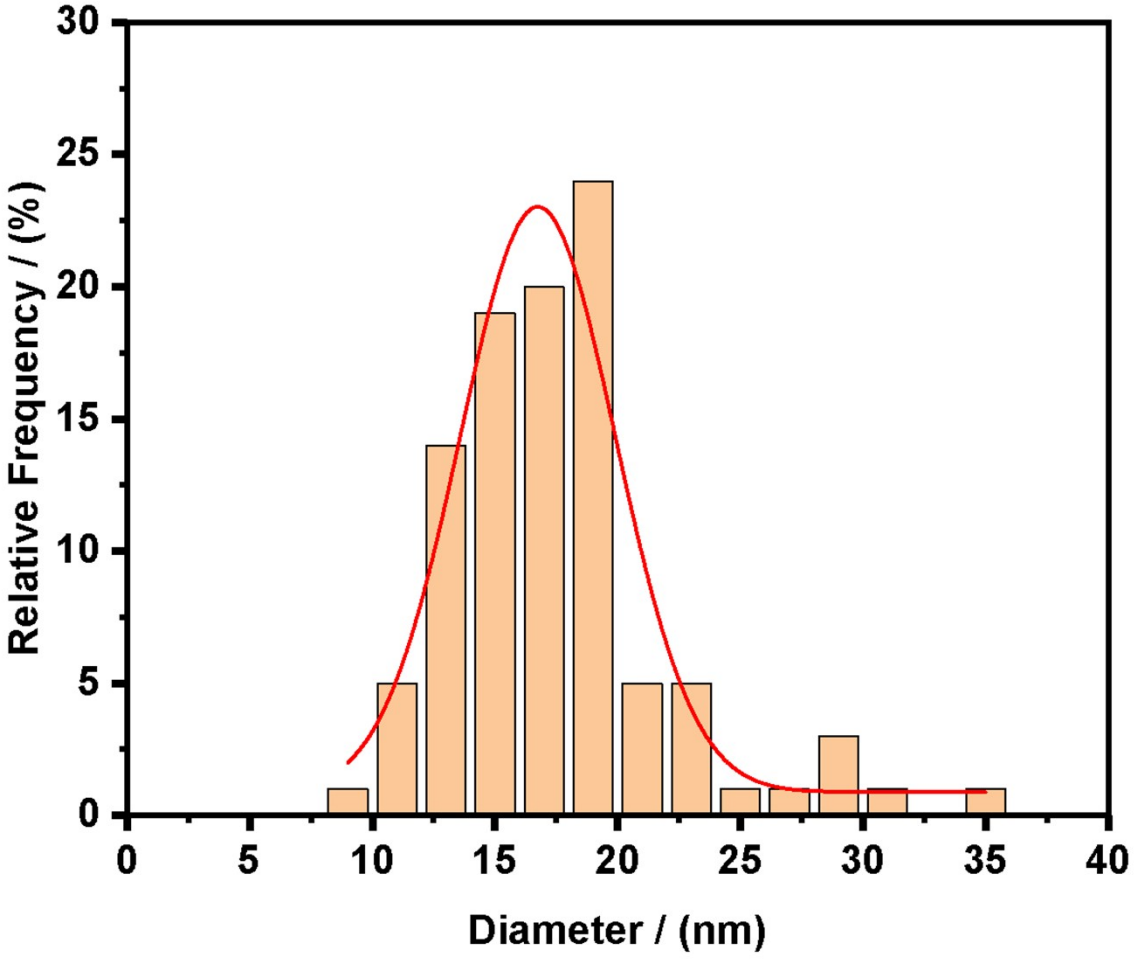

Figure S1. Diameter distribution of CuS-SnS.

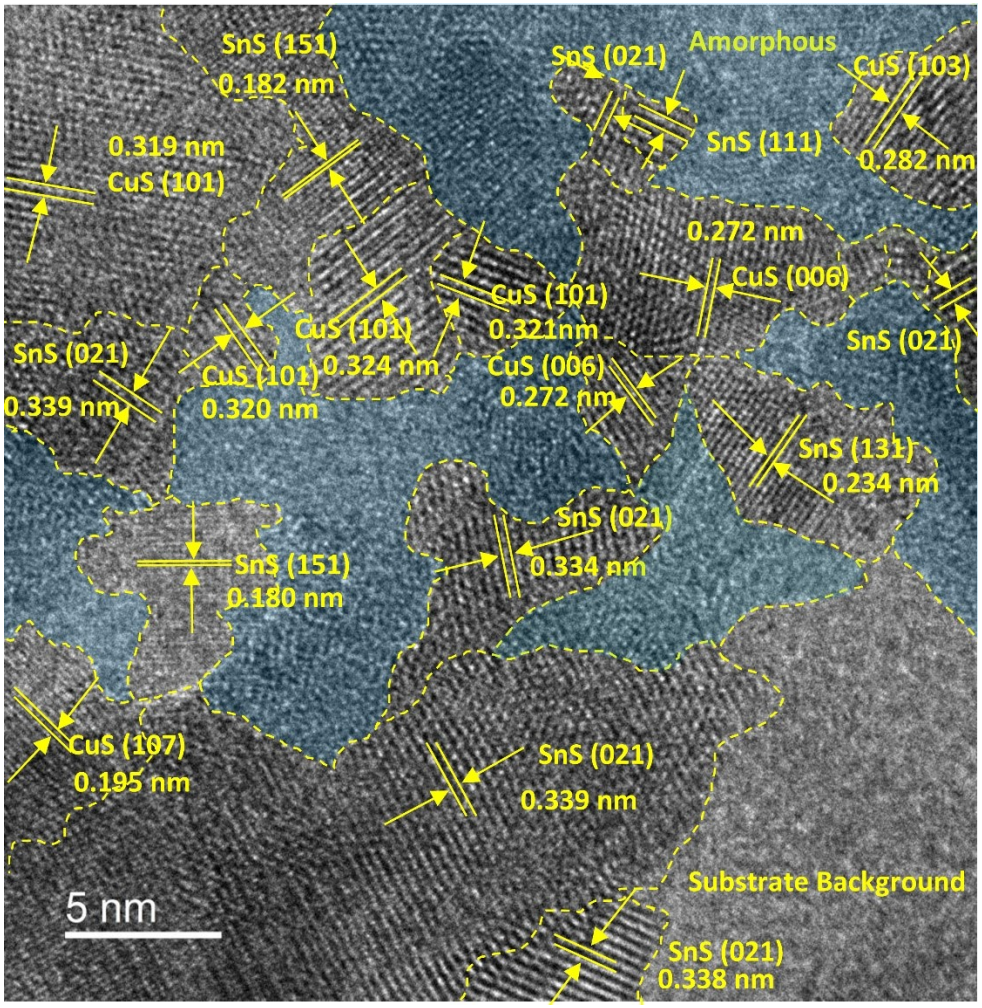

Figure S2. Identification of selected grains in Fig. 1d.

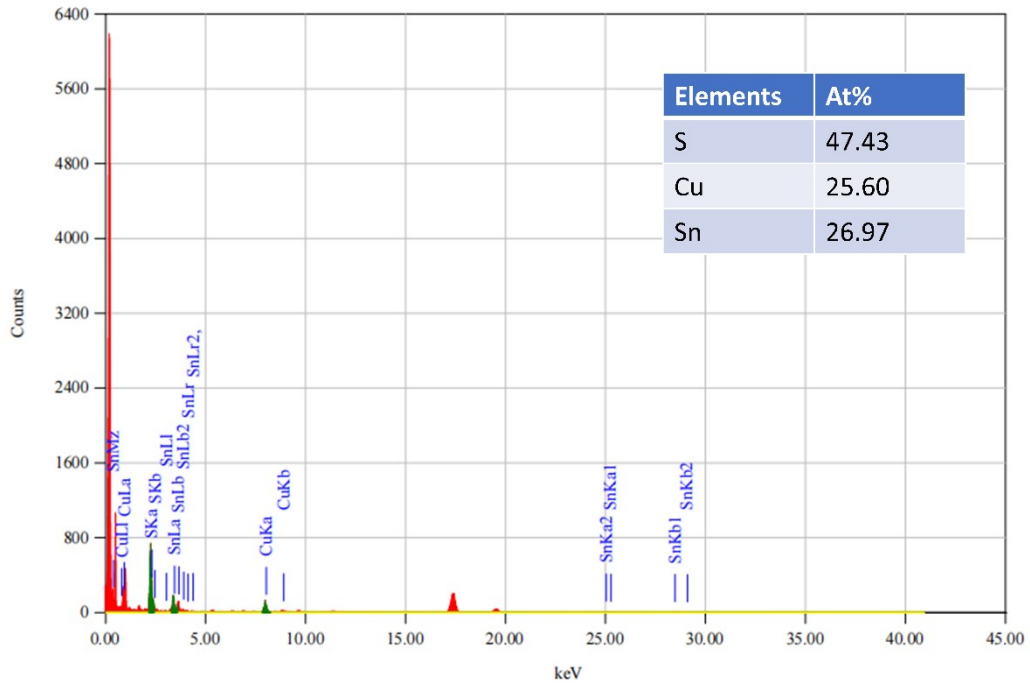

Figure S3. TEM-EDS spectrum of CuS-SnS.

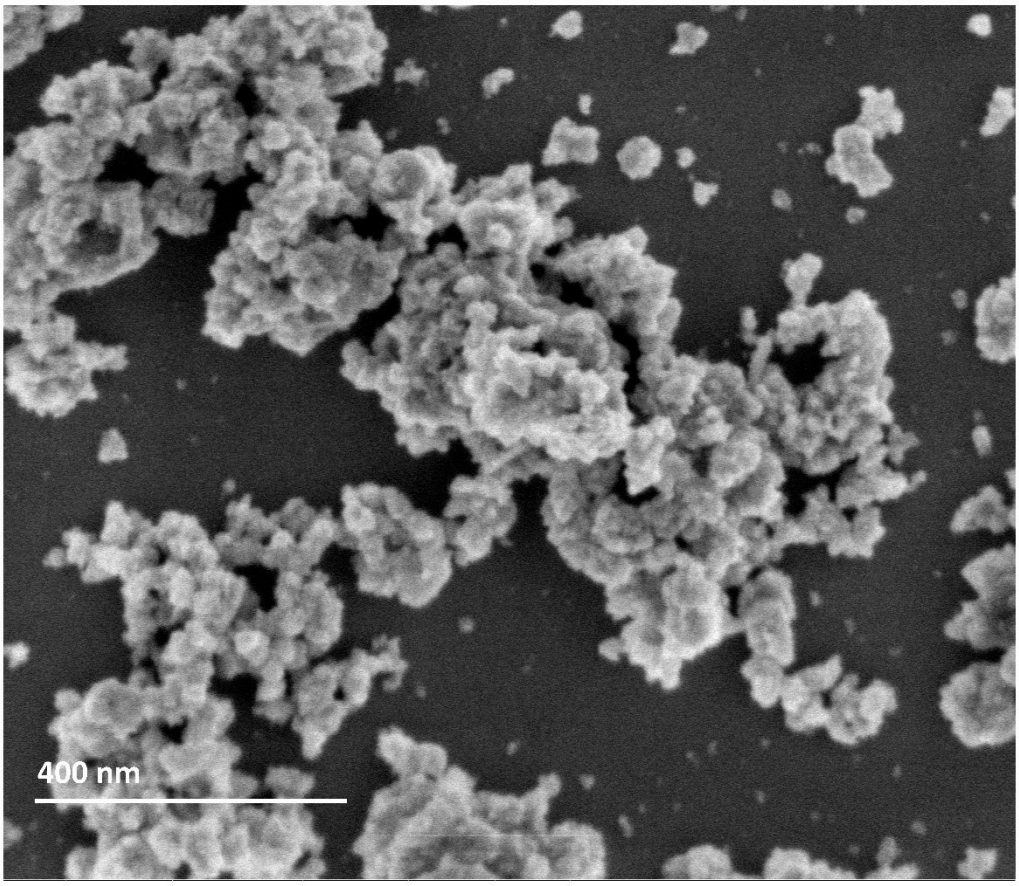

Figure S4. SEM image of CuS.

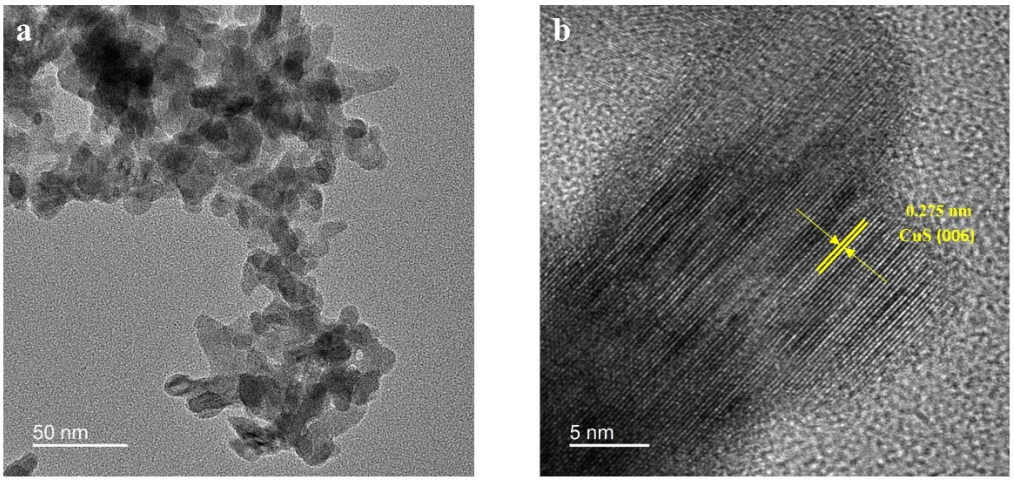

Figure S5. (a) TEM image of CuS, (b) HRTEM image of CuS.

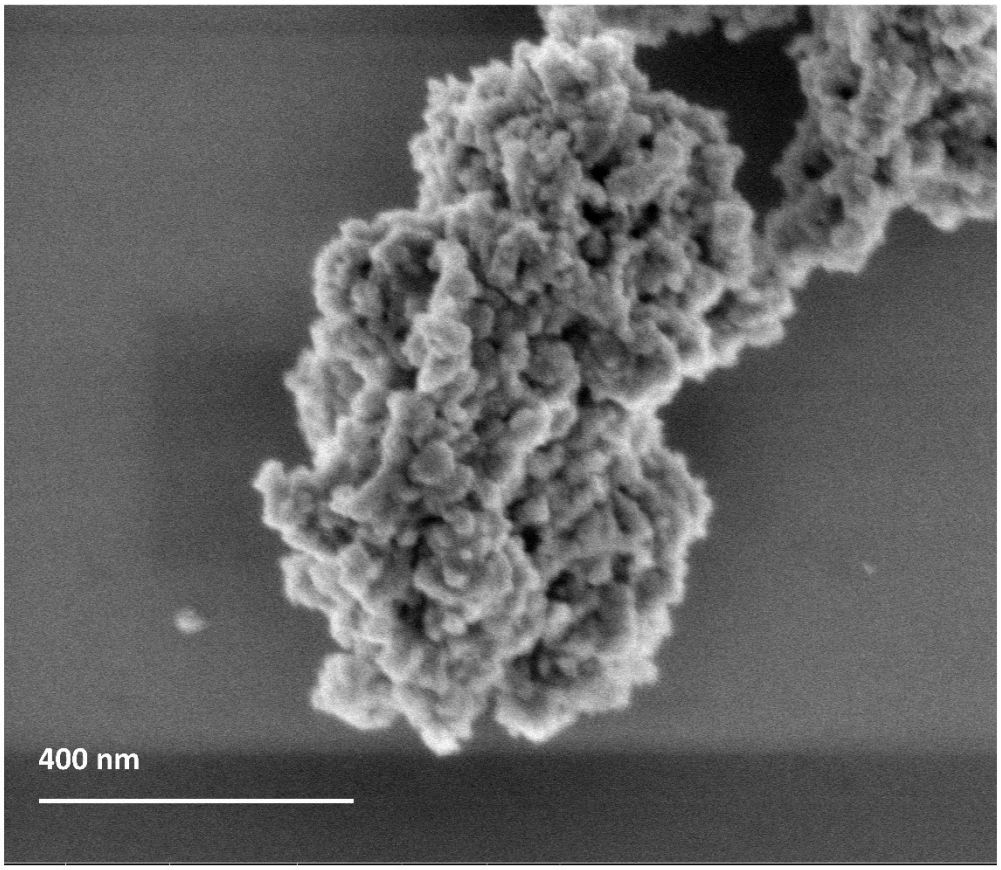

Figure S6. SEM image of SnS.

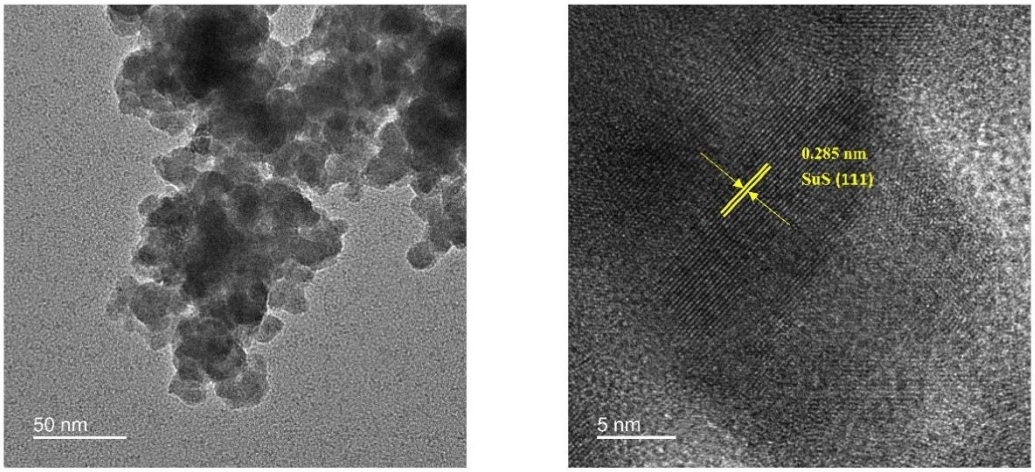

Figure S7. (a) TEM image of SnS, (b) HRTEM image of SnS.

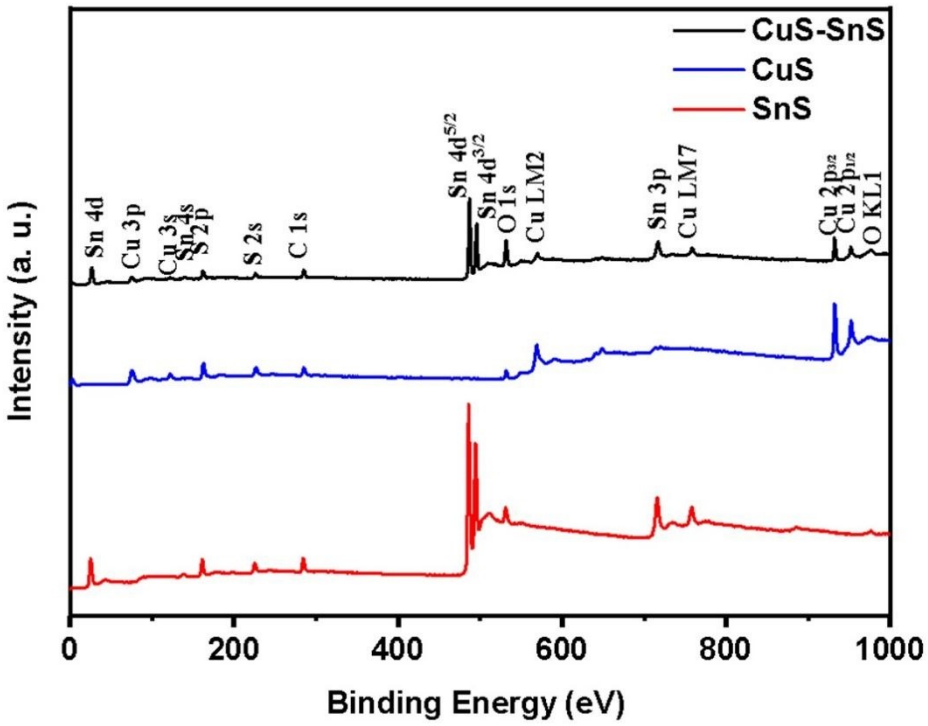

Figure S8. XPS survey spectra of CuS, SnS and CuS-SnS.

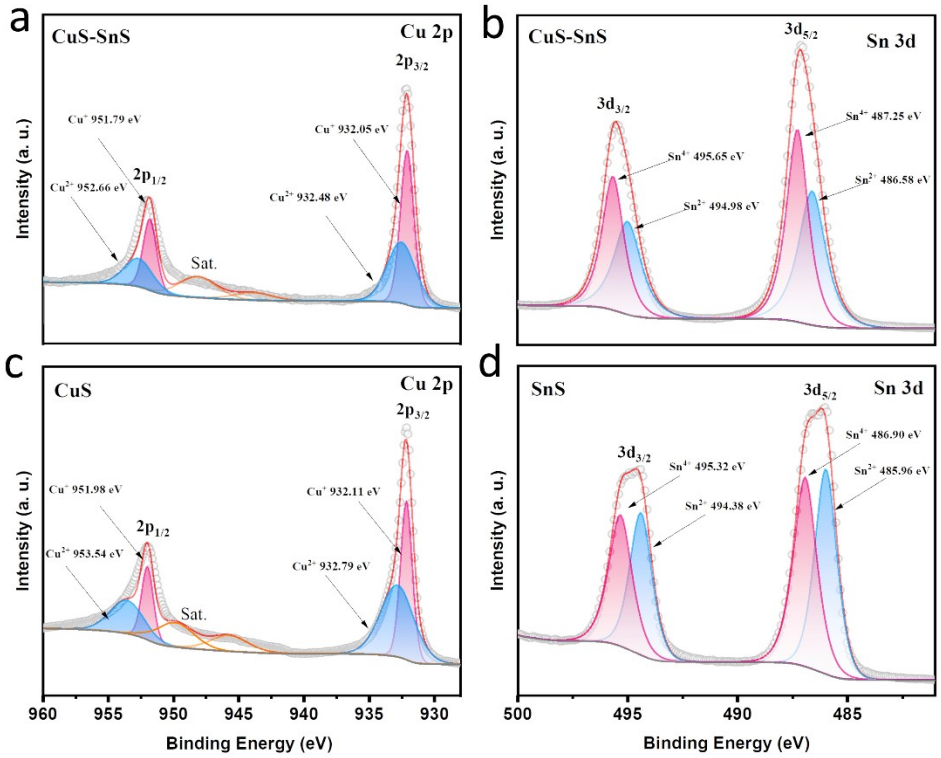

Figure S9. (a) Cu 2p XPS spectrum, (b) Sn 3d XPS spectrum of CuS-SnS. (c) Cu 2p XPS spectrum of CuS. (d) Sn 3d XPS spectrum of SnS.

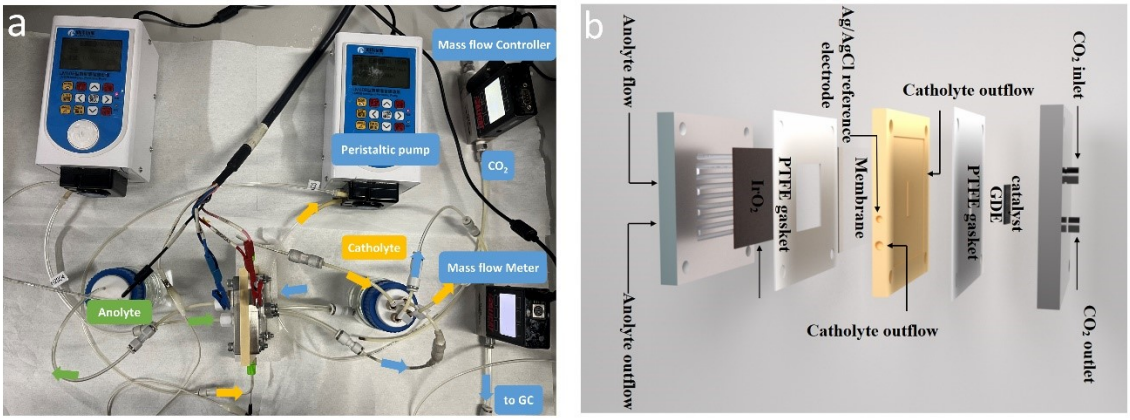

Figure S10. (a) The photograph of CO_2RR electrolysis system. (b) Schematic illustration of a customized flow cell electrolyzer.

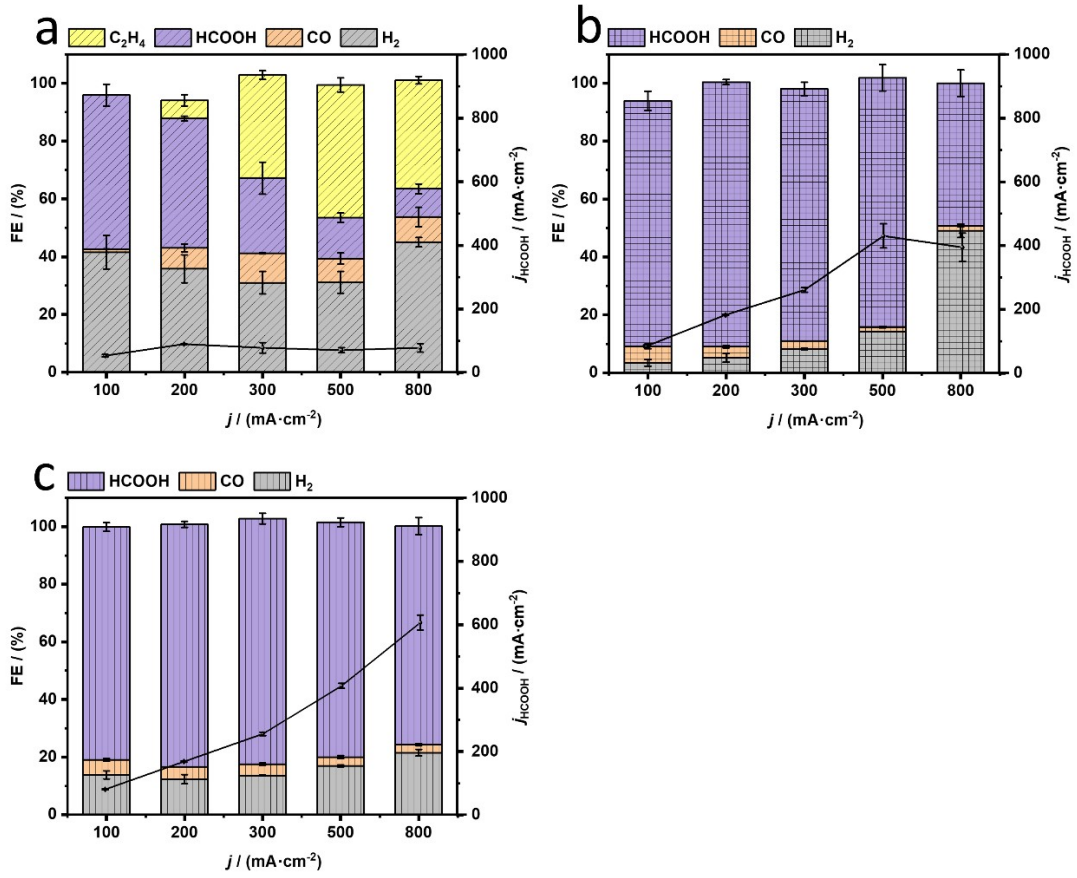

Figure S11. FEs of products and j_{HCOOH} for the (a) CuS, (b) SnS, and (c) CuS+SnS catalysts in 1 M $KHCO_3$ solution at current densities of 100 to 800 mA cm^{-2}.

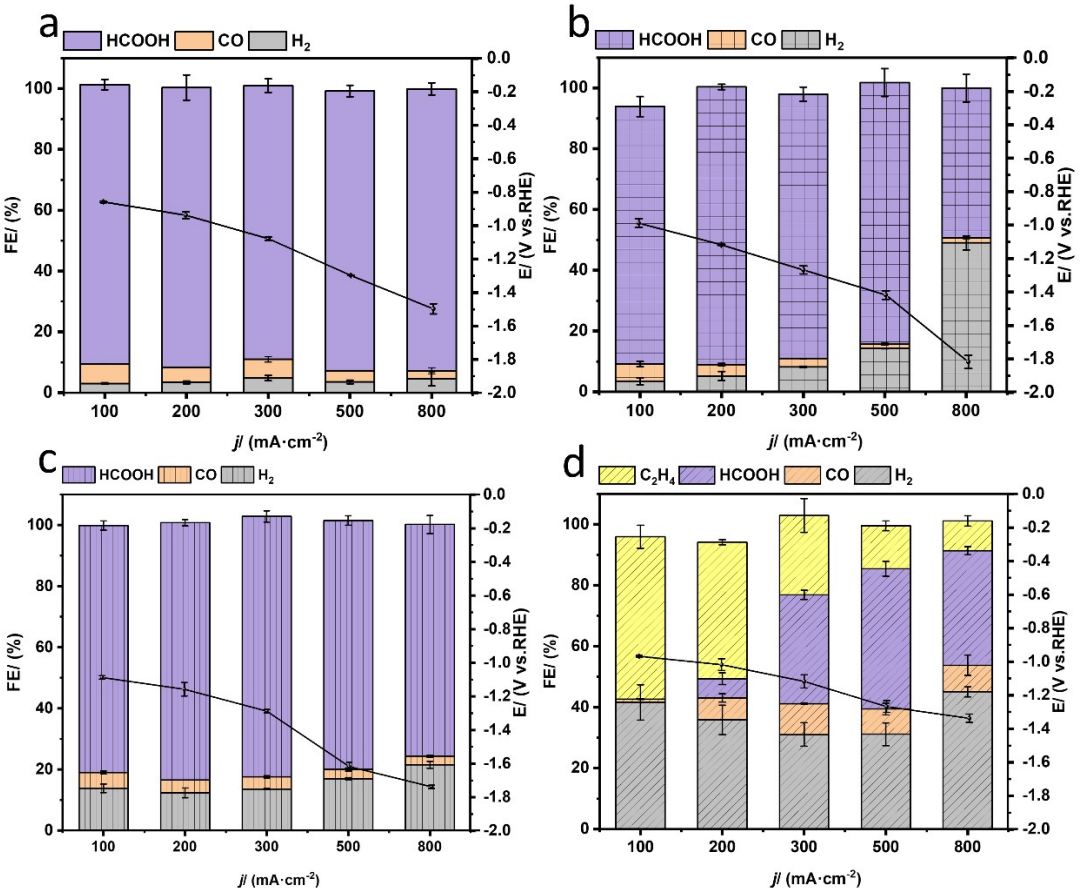

Figure S12. FEs of products and potentials vs. RHE for the (a) CuS, (b) SnS, and (c) CuS+SnS catalysts in 1 M $KHCO_3$ solution at current densities of 100 to 800 mA cm^{-2}.

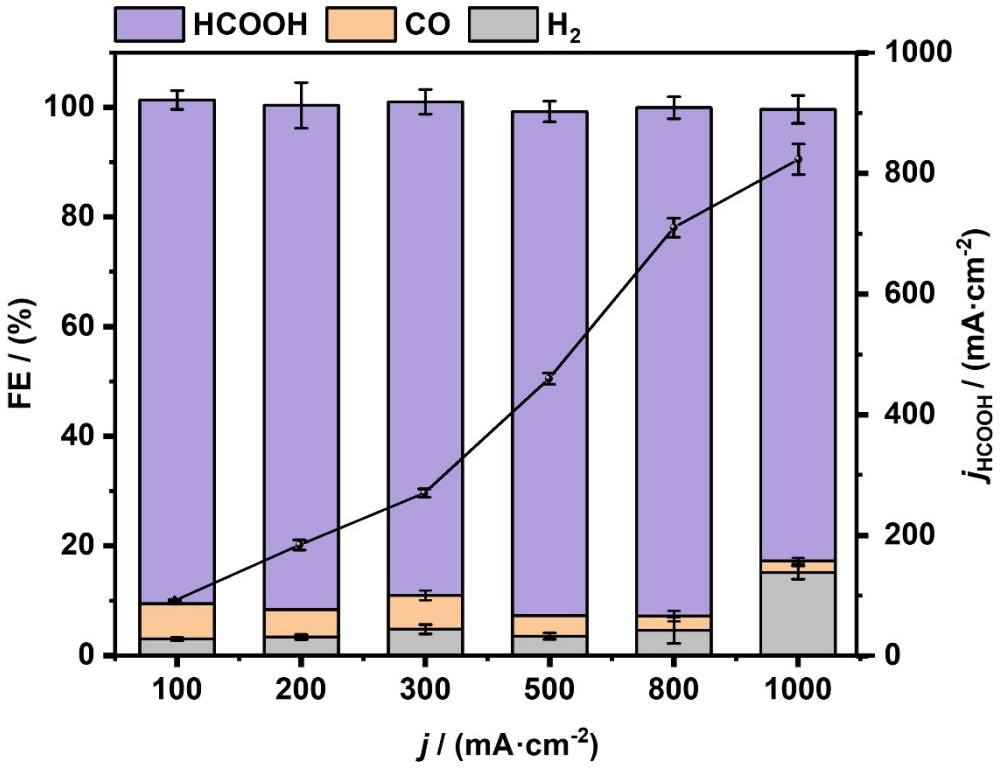

Figure S13. FEs of products and j_{HCOOH} for the CuS-SnS catalyst in 1 M $KHCO_3$ solution at current densities of 100 to 1000 mA cm^{-2}.

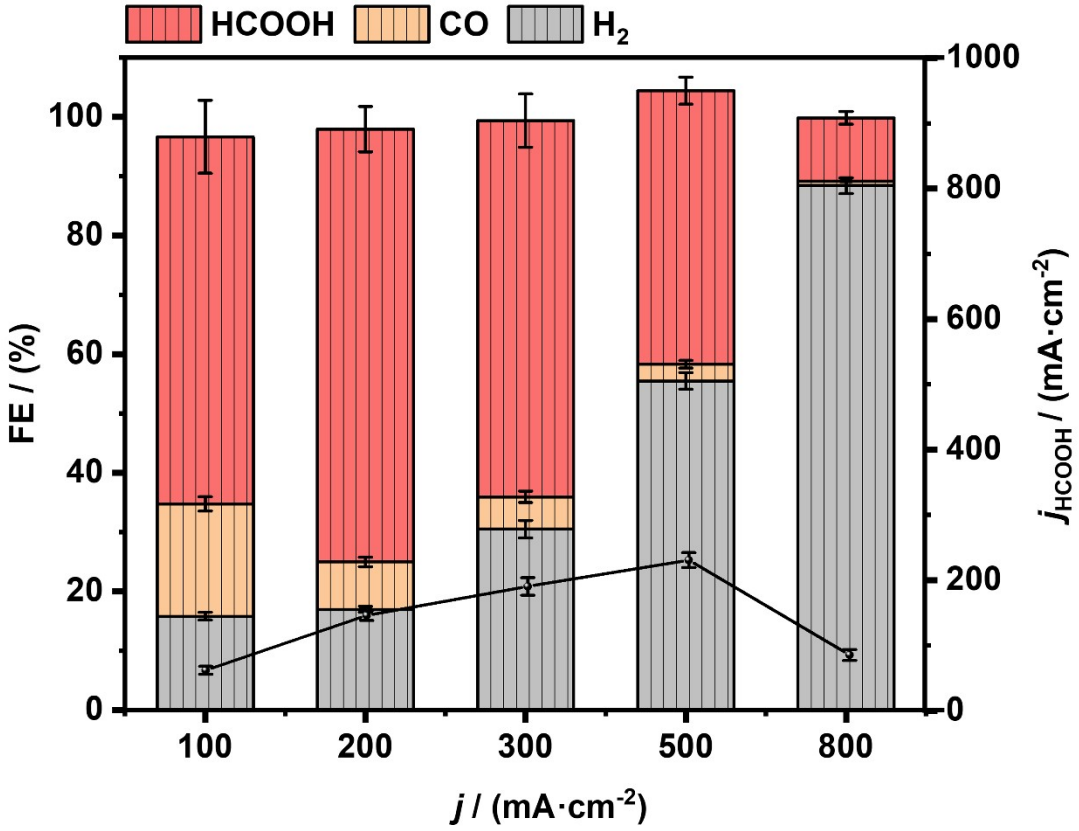

Figure S14. FEs of products and j_{HCOOH} for the CuS+SnS catalyst in 0.05 M H_2SO_4 and 0.5 M K_2SO_4 mixed solution at current densities of 100 to 800 mA cm^{-2}.

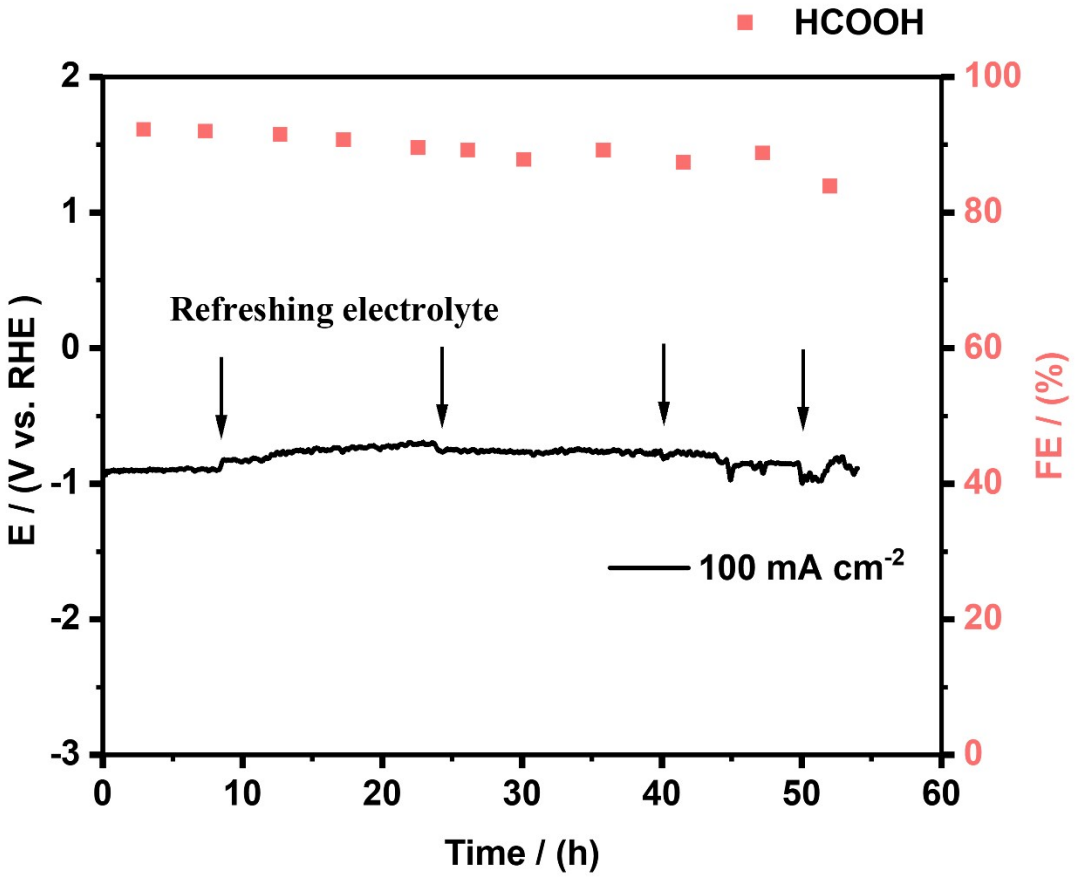

Figure S15. Stability test over a span of 50 h at a total current density of 100 mA cm^{-2} in 0.05 M H_2SO_4 and 0.5 M K_2SO_4 mixed solution.

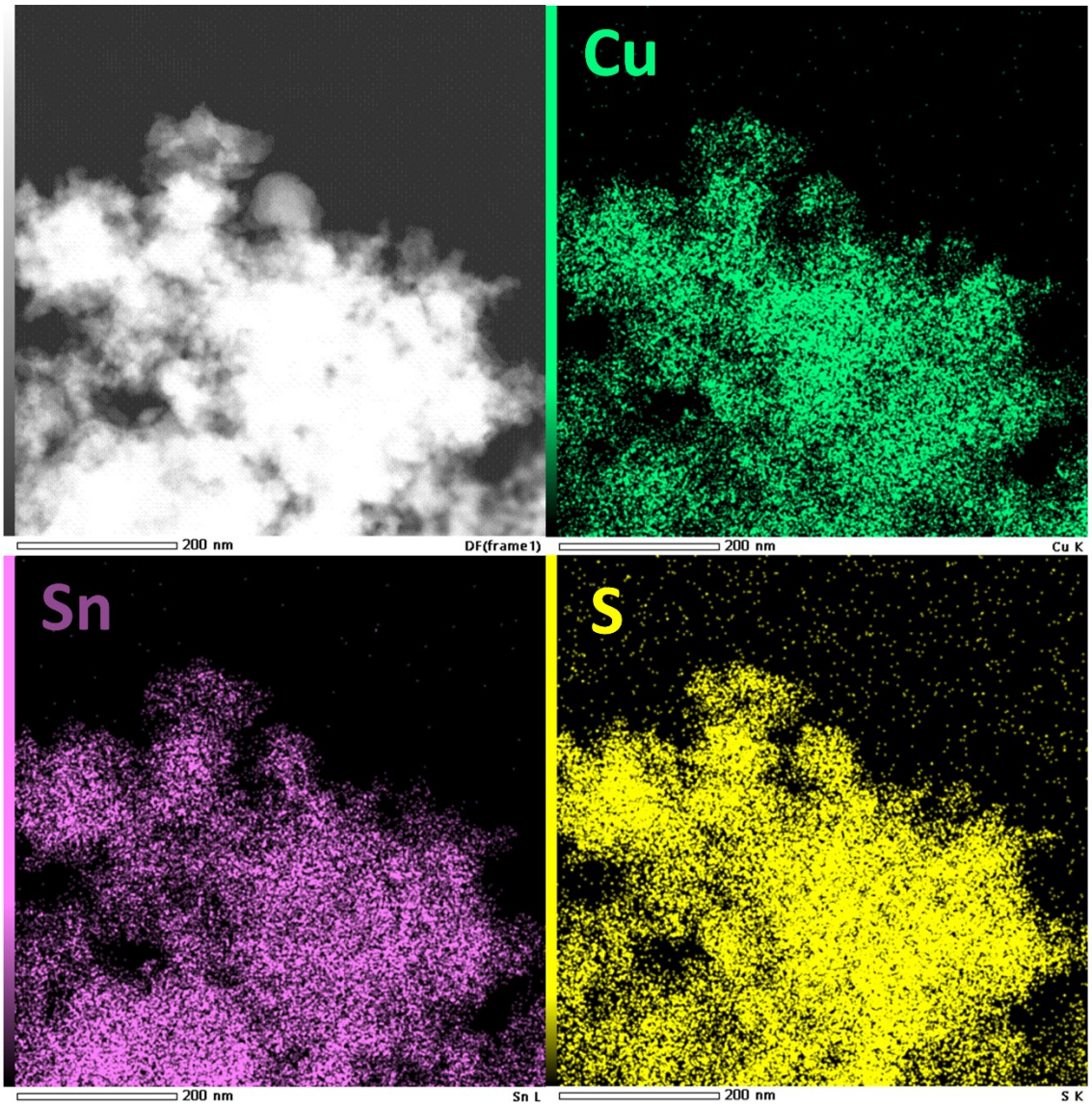

Figure S16. Element mappings of CuS-SnS catalyst after 1-h CO_2RR test at 100 mA cm^{-2}.

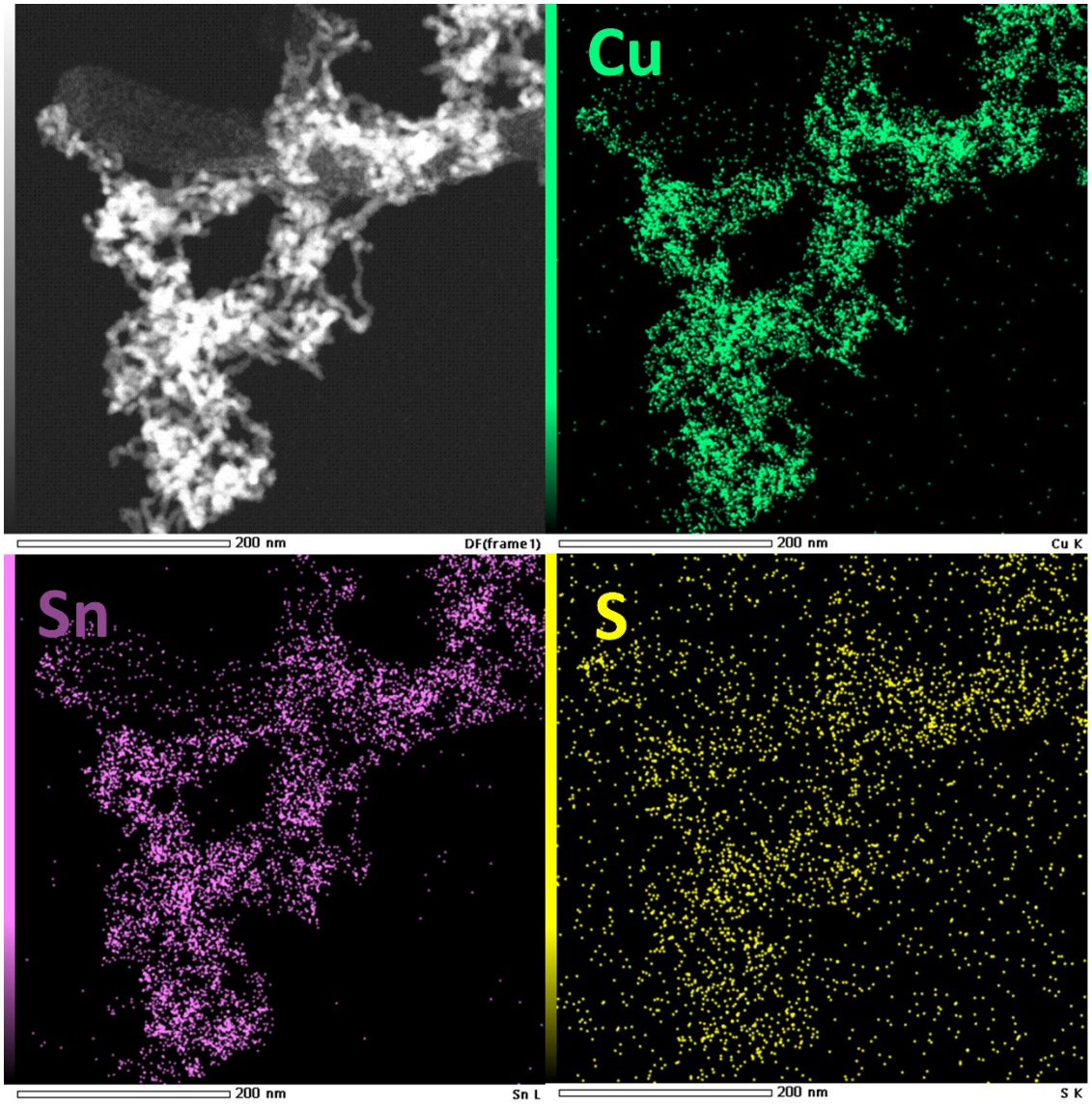

Figure S17. Element mappings of CuS+SnS catalyst after 1-h CO_2RR test at 100 mA cm^{-2}.

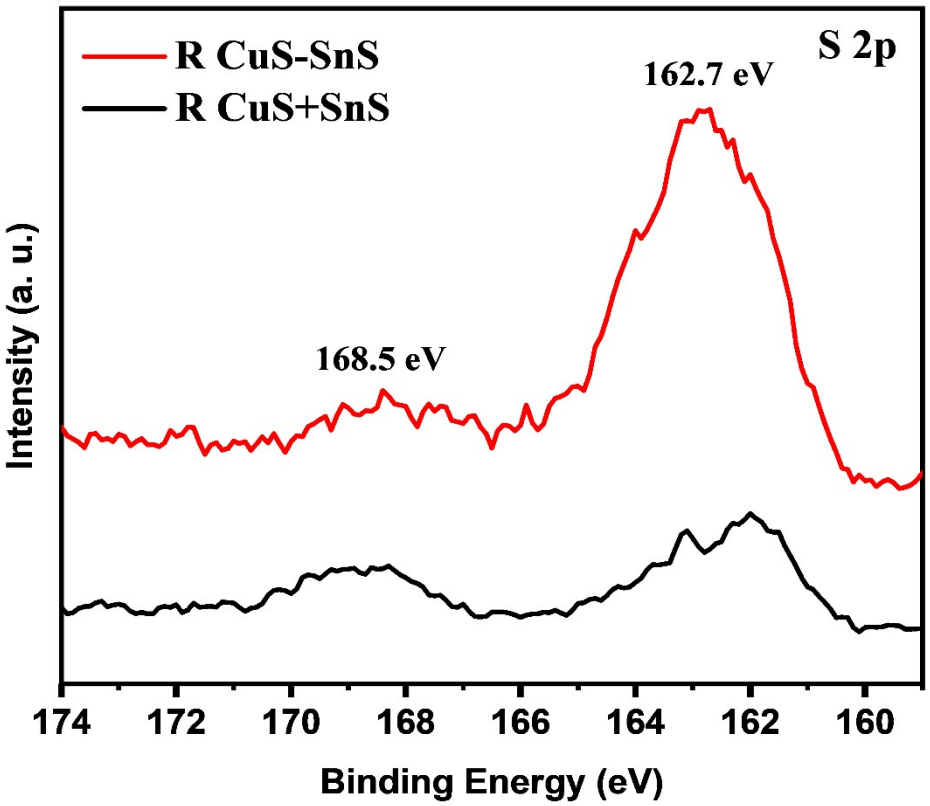

Figure S18. Ex situ XPS S 2p spectra of the CuS-SnS and CuS+SnS catalysts after 1-h CO_2RR test at 100 mA cm^{-2}. The S 2p spectra display characteristic peaks at 168.5 eV and 162.7 eV, corresponding to the S elements in Nafion binder and catalysts, respectively.[7] The Nafion binder used in this post-test XPS characterization, instead of DM XA-9, is employed as a internal standard for S element quantification.

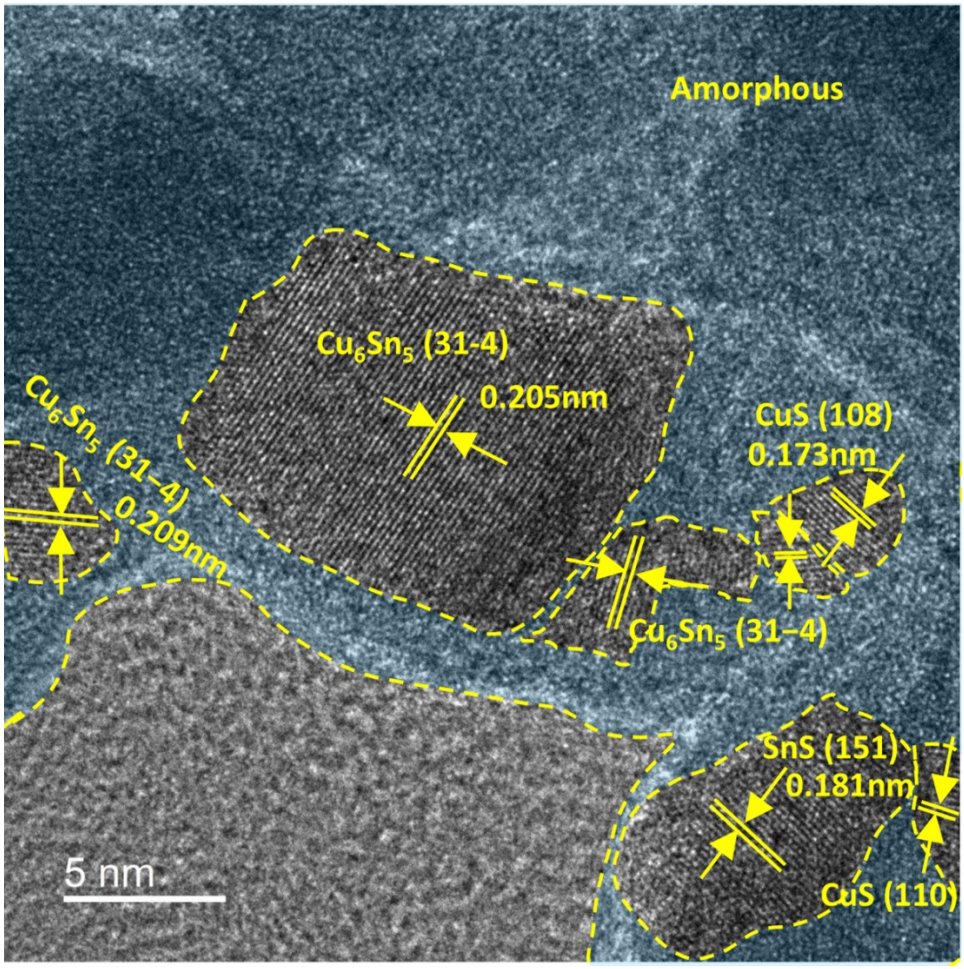

Figure S19. HRTEM image of CuS-SnS catalyst after 1-h CO_2RR test at 100 mA cm^{-2}.

.

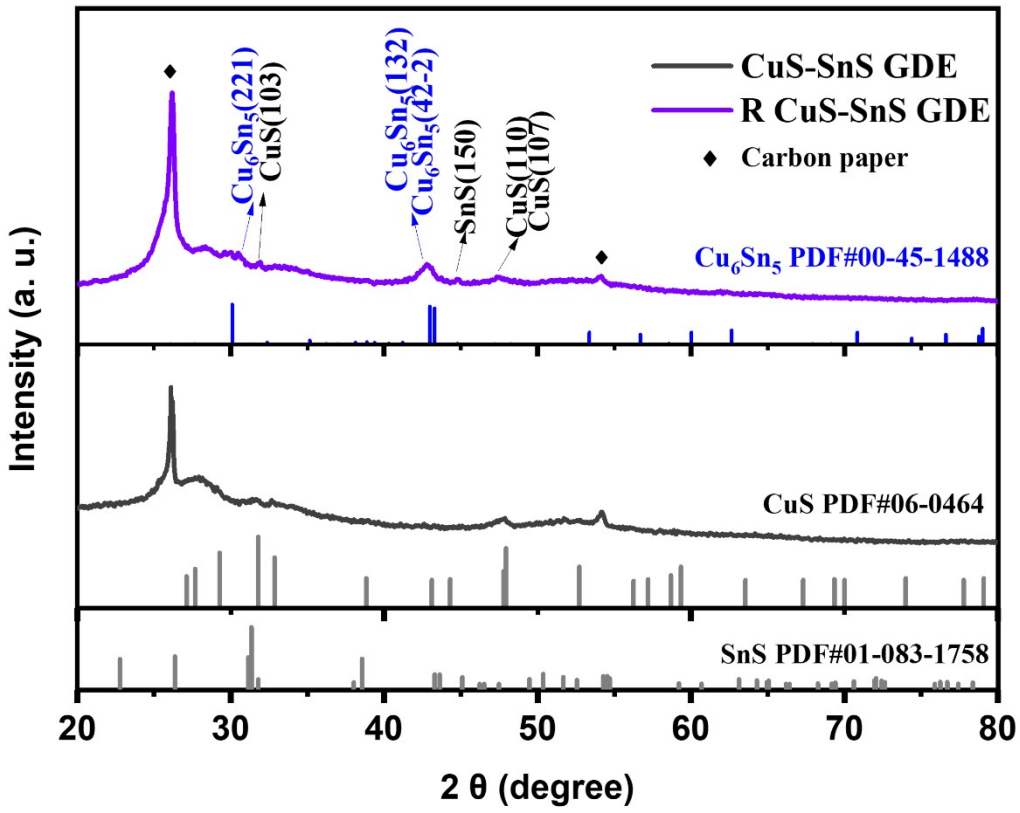

Figure S20. XRD patterns of the pristine CuS-SnS GDE and CuS-SnS GDE after 1-h CO_2RR test at 100 mA cm^{-2}.

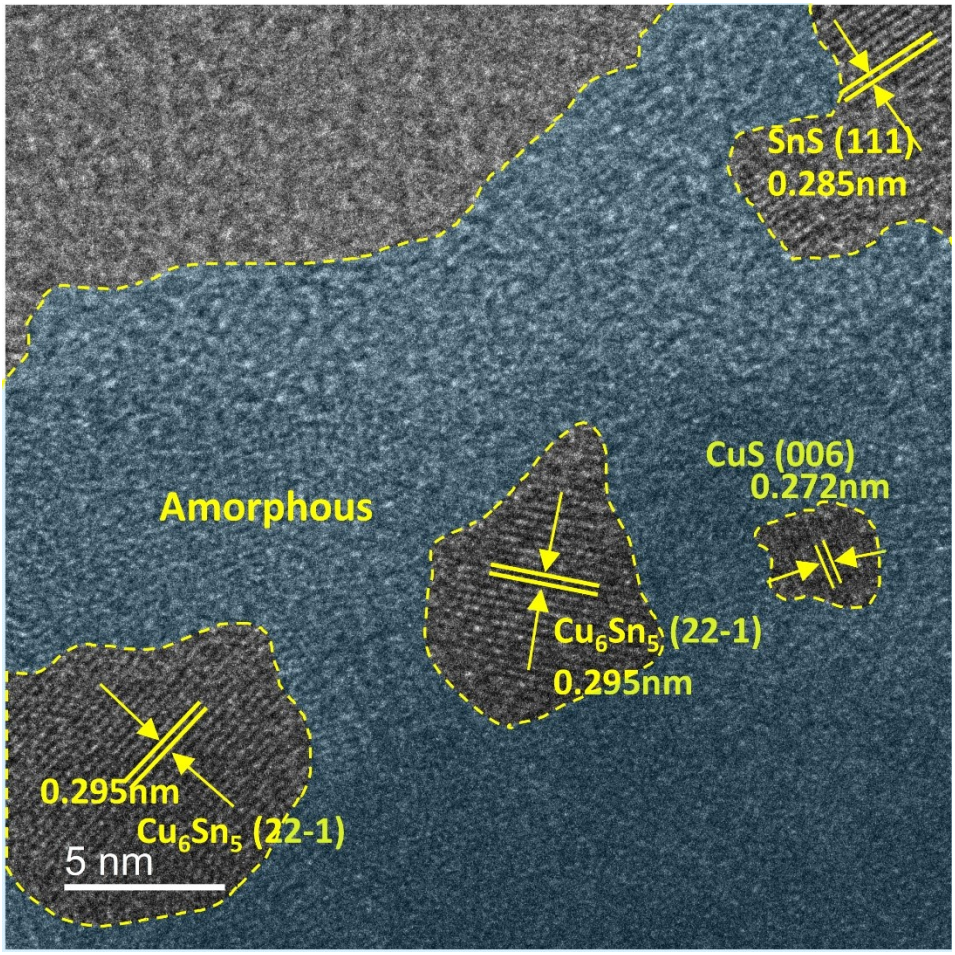

Figure S21. HRTEM image of CuS-SnS catalyst after 50-h CO_2RR test at 100 mA cm^{-2}.

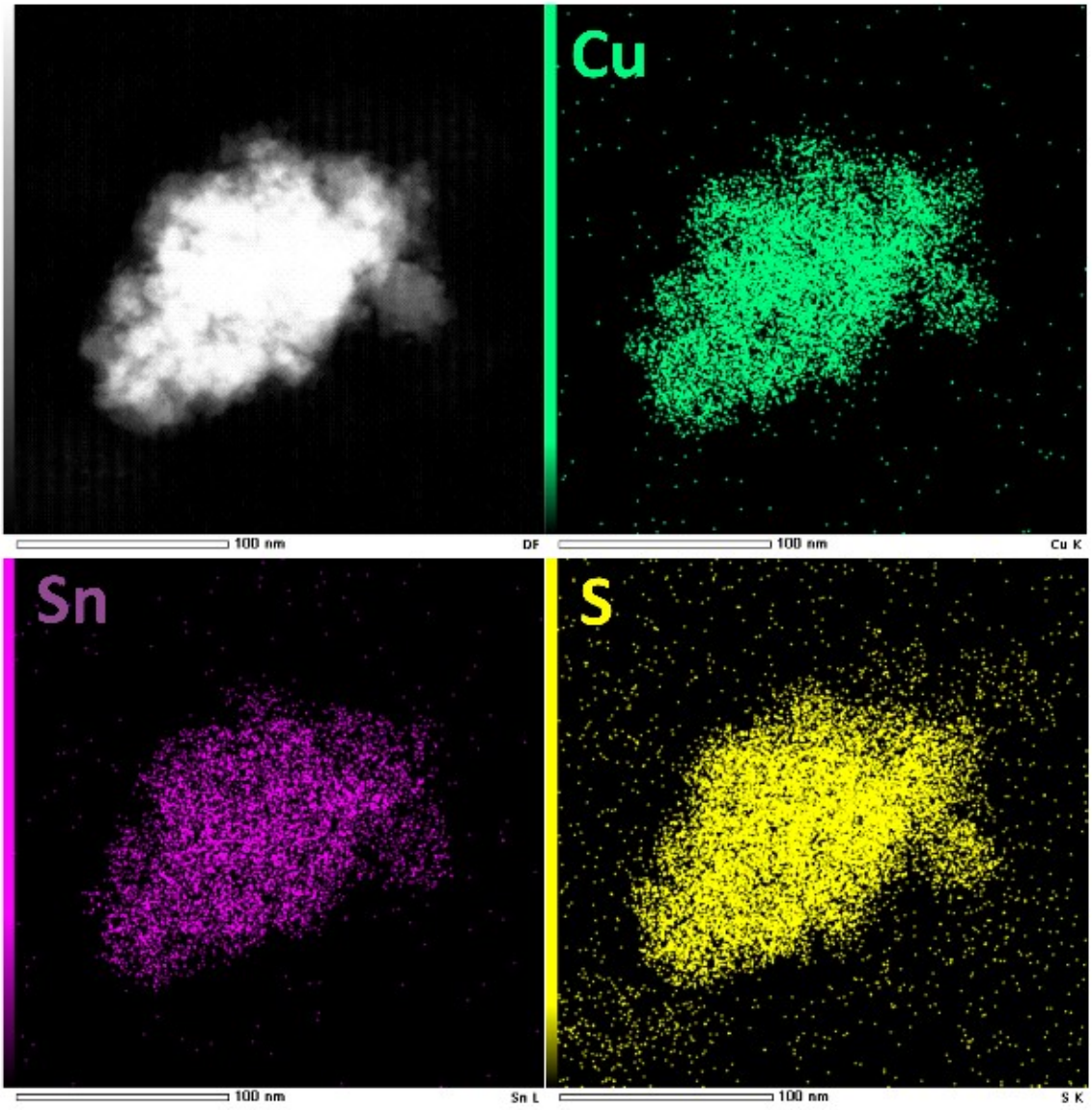

Figure S22. XRD Element mappings of CuS-SnS catalyst after 50-h CO_2RR test at 100 mA cm^{-2}.

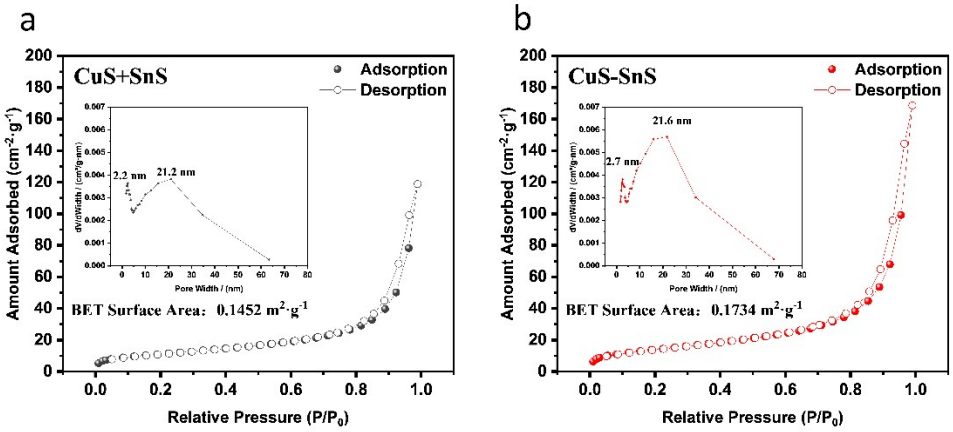

Figure S23. The N_2 adsorption-desorption isotherm and pore volume distribution of the (a) CuS+SnS and (b) CuS-SnS catalysts at 77 K

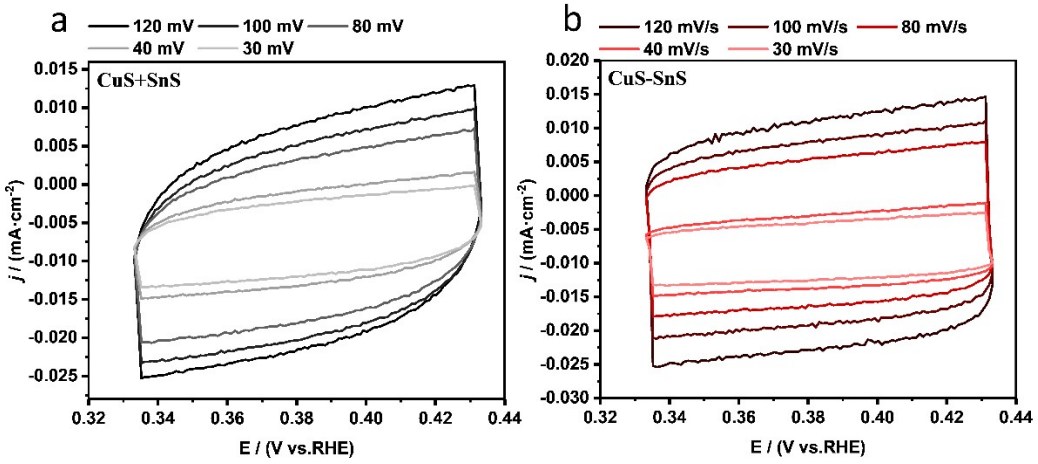

Figure S24. Double-layer charging current plotted against the CV scan rate for the three electrodes. CVs of (a) CuS+SnS and (b) CuS-SnS catalysts with different scan rate.

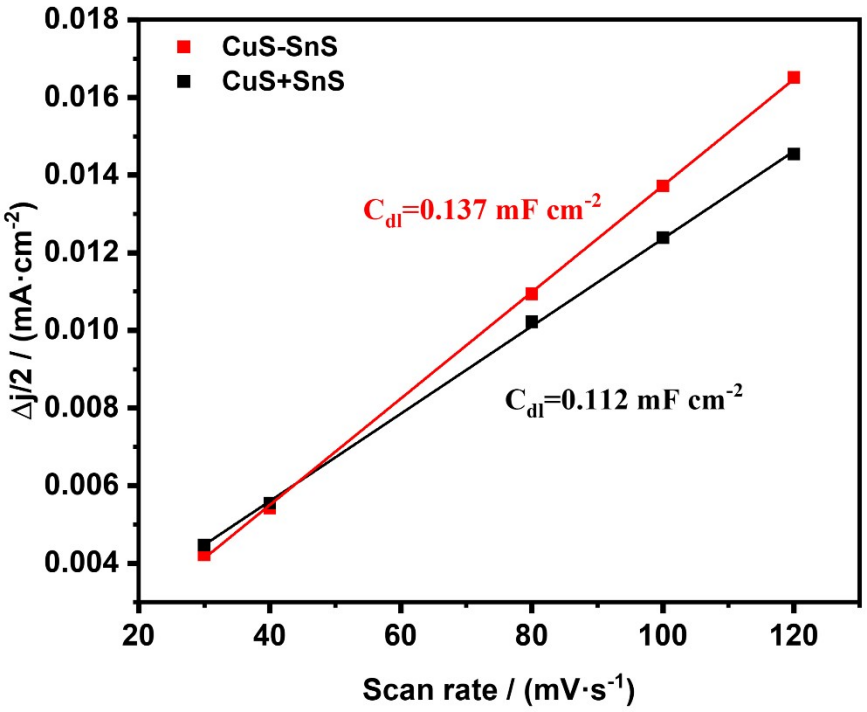

Figure S25. Charge current density differences (Δj/2) for CuS+SnS and (b) CuS-SnS catalysts plotted against scan rate.

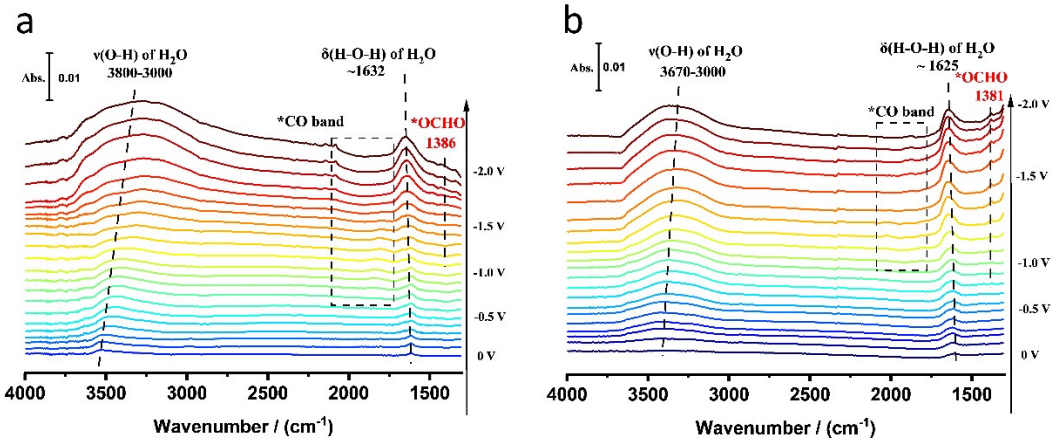

Figure S26. In situ ATR-SEIRA spectra (1300-4000 cm^{-1}) on (a) CuS-SnS and (b) CuS+SnS under CO_2RR conditions.

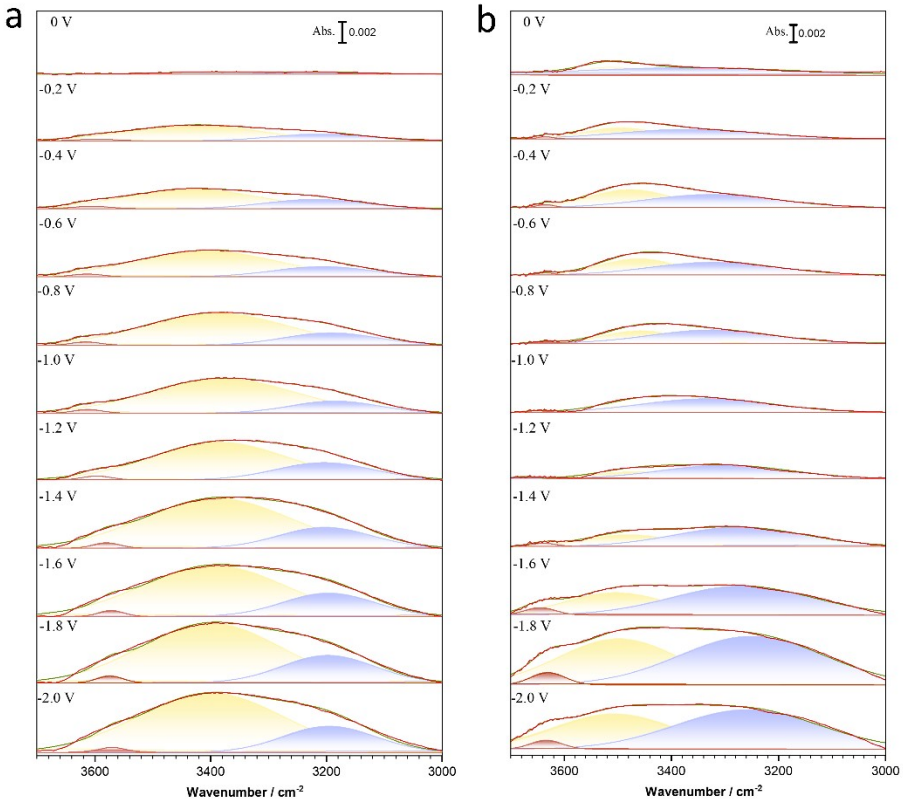

Figure S27. Deconvolution of ν(O-H) of H_2O bands on (a) CuS-SnS and (b) CuS+SnS.

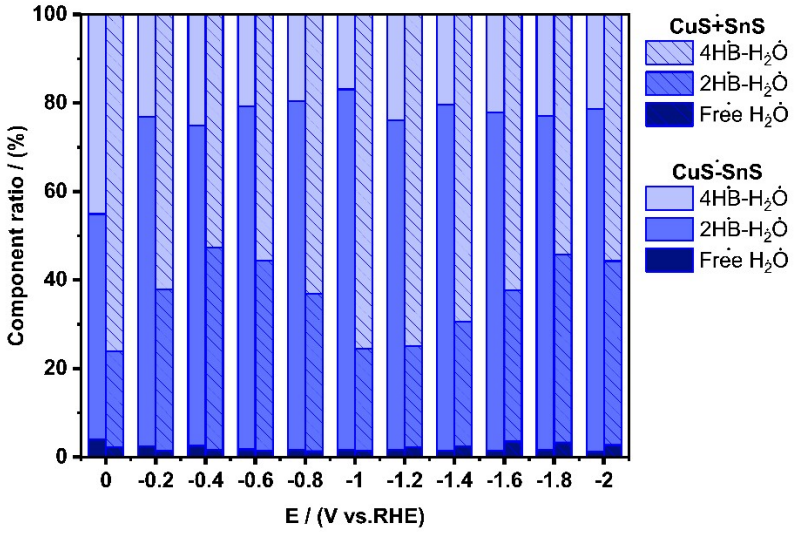

Figure S28. The percentage distribution of different H_2O components on CuS-SnS and CuS+SnS.

Notes and references

1 H. Schichlein, A. C. Müller, M. Voigts, A. Krügel and E. Ivers-Tiffée, *J. Appl. Electrochem.*, 2002, **32**, 875-882.

2 J. Weese, *Comput. Phys. Commun.*, 1992, **69**, 99-111.

3 F. Dion and A. Lasia, *J. Electroanal. Chem.*, 1999, **475**, 28-37.

4 M. Nohl, G. Raut, S. E. Wolf, T. Duyster, L. Dittrich, I. C. Vinke, R.-A. Eichel and L. G. J. De Haart, *ECS Transactions*, 2021, **103**, 1403.

5 M. Braig and R. Zeis, *J. Power Sources*, 2023, **576**, 233203.

6 T. H. Wan, M. Saccoccio, C. Chen and F. Ciucci, *Electrochim. Acta*, 2015, **184**, 483-499.

7 Y. Wang, H. Xu, Y. Liu, J. Jang, X. Qiu, E. P. Delmo, Q. Zhao, P. Gao and M. Shao, *Angew. Chem. Int. Ed.*, 2024, **63**, e202313858.